
1 **The single-particle mixing state and cloud scavenging of black carbon: a**
2 **case study at a high-altitude mountain site in southern China**

3

4 Guohua Zhang ¹, Qin hao Lin ^{1,2}, Long Peng ^{1,2}, Xinhui Bi ^{1,*}, Duohong Chen ³, Mei Li ^{4,5}, Lei
5 Li ^{4,5}, Fred J. Brechtel ⁶, Jianxin Chen ⁷, Weijun Yan ⁷, Xinming Wang ¹, Ping'an Peng ¹,
6 Guoying Sheng ¹, Zhen Zhou ^{4,5}

7

8 ¹State Key Laboratory of Organic Geochemistry and Guangdong Key Laboratory of
9 Environmental Resources Utilization and Protection, Guangzhou Institute of Geochemistry,
10 Chinese Academy of Sciences, Guangzhou 510640, PR China

11 ²University of Chinese Academy of Sciences, Beijing 100039, PR China

12 ³ State Environmental Protection Key Laboratory of Regional Air Quality Monitoring,
13 Guangdong Environmental Monitoring Center, Guangzhou 510308, PR China

14 ⁴ Institute of Mass Spectrometer and Atmospheric Environment, Jinan University, Guangzhou
15 510632, PR China

16 ⁵ Guangdong Provincial Engineering Research Center for on-line source apportionment system
17 of air pollution, Guangzhou 510632, PR China

18 ⁶Brechtel Manufacturing Inc., Hayward, 94544, California, USA

19 ⁷Shaoguan Environmental Monitoring Center, Shaoguan 512026, PR China

20

21 Correspondence should be addressed to Xinhui Bi (bixh@gig.ac.cn)

22 **Highlights**

23 ● In situ investigation on the cloud scavenging of BC in company with the mixing state was
24 first reported in China.

25 ● The number fraction of scavenged BC-containing particles is close to that of all the
26 measured particles.

27 ● BC-containing particles with higher fractions of organics were scavenged relatively less
28 than those with higher fractions of sulfate.

29

30 **Abstract**

31 In the present study, a ground-based counterflow virtual impactor (GCVI) was used to
32 sample cloud droplet residual (cloud RES) particles, while a parallel PM_{2.5} inlet was used to
33 sample cloud-free or cloud interstitial (cloud INT) particles. The mixing state of black carbon
34 (BC)-containing particles and the mass concentrations of BC in the cloud-free, RES and INT
35 particles were investigated using a single particle aerosol mass spectrometer (SPAMS) and
36 two aethalometers, respectively, at a mountain site (1690 m a.s.l.) in southern China. The
37 measured BC-containing particles were extensively internally mixed with sulfate, and were
38 scavenged into cloud droplets (0.05–0.45) to a similar (or slightly lower) extent as all the
39 measured particles (0.07–0.6) over the measured size range of 0.1–1.6 μm. The results indicate
40 the preferential activation of larger particles and/or that the production of secondary
41 compositions shifts the BC-containing particles towards larger sizes. BC-containing particles
42 with an abundance of both sulfate and organics were scavenged less than those with sulfate but
43 limited organics, implying the importance of the mixing state on the incorporation of
44 BC-containing particles into cloud droplets. The mass scavenging efficiency of BC with an
45 average of 33% was similar for different cloud events independent of the air mass. This is the
46 first time that both the mixing state and cloud scavenging of BC in China have been reported.
47 Our results would improve the knowledge on the concentration, mixing state, and cloud
48 scavenging of BC in the free troposphere.

49

50 **Keywords:** black carbon, cloud droplet residual particles, mixing state, cloud scavenging,
51 interstitial particle

52 **1 Introduction**

53 Black carbon (BC), also known as soot or elemental carbon, is primarily emitted from
54 incomplete combustion processes (Bond et al., 2013; Petzold et al., 2013). Fresh
55 BC-containing particles are generally hydrophilic due to the presence of thin coatings of
56 inorganic or organic materials (Zuberi et al., 2005), and during transport they become more
57 hydrophilic when further coated through coagulation, condensation and photochemical
58 oxidation (Zuberi et al., 2005; Zaveri et al., 2010; Matsui, 2016). Hydrophilic BC-containing
59 particles can act as cloud condensation nuclei (CCN) and thus modify cloud microphysical
60 properties (Straub et al., 2012; Schroder et al., 2015; Roth et al., 2016). The increase in CCN
61 activity enhances the in-cloud scavenging of BC and thus reduces its lifetime (Zaveri et al.,
62 2010). Aerosol-cloud interactions represent one of the largest uncertainties in our current
63 understanding of human-induced climate forcing (McFiggans et al., 2006; Andreae and
64 Rosenfeld, 2008). Therefore, a more comprehensive understanding of how aerosol particles
65 form cloud droplets is required in order to reduce the uncertainty of the impacts of aerosols
66 on the climate (Furutani et al., 2008).

67 The abilities of particles to act as CCN are largely controlled by their sizes and chemical
68 compositions or mixing state (Dusek et al., 2006; Cubison et al., 2008; Kammermann et al.,
69 2010; Baustian et al., 2012; Ching et al., 2012). Larger aerosol particles were found to be
70 more easily scavenged into cloud droplets (Drewnick et al., 2007). Zhou et al. (2009) found
71 higher scavenging rates for sulfate, nitrate and BC than those for organics at Mount Tai in
72 northern China. At the same site, 92% of the cloud residual particles were attributed to

73 sulfate-related salts (Li et al., 2011b). On the other hand, the chemical compositions of the
74 original CCN could be altered after the evaporation of the cloud droplets through the
75 effective formation of secondary aerosol compositions during cloud processing (Hayden et
76 al., 2008; Herrmann et al., 2015; Roth et al., 2016). The mixing state of BC-containing
77 particles is of high concern, since their activation as CCN is primarily attributed to the
78 presence of secondary coatings (Lambe et al., 2015; Schroder et al., 2015). Additionally, the
79 mixing state of BC-containing particles is complex and constantly changing in the
80 atmosphere, and they are highly influenced by the particle size, sources, the formation of
81 secondary species and transport processes (Cahill et al., 2012; Healy et al., 2012; Zhang et
82 al., 2014).

83 Recent in situ studies of cloud droplets have provided the most direct information on the
84 incorporation of BC into clouds. The mass scavenging efficiency was observed to be in a
85 range of 33–74% for BC, which was higher with increasing particle sizes at the Puy de Dome
86 (1465 m a.s.l.), France (Sellegrì et al., 2003). It ranged from 13% to 50% corresponding to
87 different air masses at a coastal Chilean hill (450 m a.s.l.) (Heintzenberg et al., 2016). Cozic
88 et al. (2007) reported a scavenging rate of BC similar to those of bulk aerosols due to its
89 internal mixing state with soluble materials. Wang et al. (2012) showed a higher scavenging
90 efficiency for BC than those for organics. Roth et al. (2016) found an enhanced contribution
91 of BC-containing particles in cloud residual particles compared to that in interstitial particles.
92 However, Zelenyuk et al. (2010) observed negligible BC in cloud droplet residual particles
93 above Alaska, USA. Therefore, an in-depth study on the composition, size and mixing state

94 of BC in cloud droplets and interstitial particles is necessary for a better understanding of the
95 interactions between BC and cloud droplets, and the influences of anthropogenic emissions
96 on cloud formation in the free troposphere.

97 Single-particle mass spectrometry (SPMS) studies on fog interstitial particles and
98 droplet residual particles were performed previously at an urban site in southern China
99 (Zhang et al., 2012; Bi et al., 2016). The predominance of BC-containing particles serving as
100 effective fog condensation nuclei highlights the important influence of anthropogenic
101 emissions on the public environment and regional climate (Bi et al., 2016). However, there
102 are no direct observations of the cloud scavenging of BC or the mixing states of cloud
103 interstitial (cloud INT) and droplet residual (cloud RES) BC-containing particles in the
104 high-altitude atmosphere or the free troposphere above China to date. Therefore, the
105 size-resolved mixing state and the scavenging efficiency of BC-containing particles were
106 investigated at a high-altitude site to further our knowledge of (1) the mixing state of
107 BC-containing particles, (2) the influence of the mixing state on the incorporation of BC
108 into cloud droplets, and (3) the influence of anthropogenic activities on cloud formation in
109 the free troposphere above southern China.

110

111 **2 Methods**

112 **2.1 Sampling setup**

113 The observations of cloud events were conducted at the National Atmospheric
114 Background Monitoring Station in Nanling of Guangdong Province, which is located on the

115 top of Mount Tianjing (24°41'56"N, 112°53'56"E, 1690 m a.s.l.) in southern China, from 16
116 to 26 Jan 2016. The average boundary layer height (<https://www.arl.noaa.gov>) at the site
117 over the study is ~280 m compared to the surrounding ground altitude (~500 m) for this
118 region. It is reasonable to consider this site sampling free tropospheric air throughout the
119 study. The site is located in a natural preserve distant from anthropogenic activities. A map
120 of the location and terrain of the site can be found elsewhere (Lin et al., 2017).

121 Aerosols were introduced into the instruments through two parallel sampling lines. The
122 first inlet is a ground-based counterflow virtual impactor (GCVI) (Model 1205, Brechtel
123 Mfg., Inc., USA) (Bi et al., 2016). The GCVI employs a compact wind tunnel upstream of
124 the CVI inlet (Model 1204) to accelerate fog and cloud droplets into the CVI inlet tip.
125 Similar methodologies have been extensively applied to collect fog/cloud RES particles (e.g.,
126 Sorooshian et al., 2013; Roth et al., 2016; van Pinxteren et al., 2016). The detail information
127 on the design of the CVI inlet and testing on the size-resolved transmission efficiency of
128 droplets can be found elsewhere (Shingler et al., 2012). The inlet cut size was set to be 8 μm ,
129 at which the transmission efficiency of droplets is 50%. The enhancement factor (EF) was
130 calculated according to the equation (Shingler et al., 2012): $EF = A_{\text{tip}} * V_{\text{air}} / q_{\text{sample}}$, where A_{tip}
131 is the area of the inlet tip where drops enter, V_{air} is wind tunnel velocity, and q_{sample} is the
132 volumetric flow rate of sampled air in the CVI inlet. A_{tip} is $1.67 \times 10^{-5} \text{ m}^2$, q_{sample} is 15 l min^{-1} ,
133 and V_{air} was set to be ~80 m/s, coincides with an EF of 5.25. Therefore, the reported mass
134 concentrations for the cloud RES particles in the following text were first divided by 5.25.
135 The sampled cloud droplets enter the evaporation chamber (with an airflow temperature of

136 40 °C), where the droplets are dried, thereby leaving behind cloud RES particles that were
137 CCN. The influence of background particles on the collection of the cloud RES particles
138 could be negligible. A test on the cloud-free air showed that the average particles number
139 concentration sampled by the GCVI was $\sim 1 \text{ cm}^{-3}$, far below the level ($\sim 2000 \text{ cm}^{-3}$) air over
140 the study (Zhang et al., 2017). A testing before measurements demonstrates that the
141 influence of background aerosols on the collection of cloud droplets could be negligible
142 (Zhang et al., 2017). The ambient inlet is a PM_{2.5} sampling line that delivers ambient
143 particles during cloud-free periods or cloud INT particles during cloud events. Cloud INT
144 particles were regarded as PM_{2.5} during the cloud events. More detailed description on the
145 sampling can be found in the companion papers (Lin et al., 2017; Zhang et al., 2017).

146 Cloud events were characterized by a sudden drop in visibility and a sharp increase in
147 the relative humidity (RH) measured by the GCVI. An upper-limit visibility threshold of 5
148 km and a lower-limit RH threshold of 95% were established to identify the cloud events and
149 trigger the sampling of the cloud RES particles.

150 An illustrative scheme of the instrumentation setup is provided in Fig. S1 in the
151 Supporting Information (SI). Downstream of the GCVI, an aethalometer (Model AE-33,
152 Magee Scientific, USA), a single particle aerosol mass spectrometer (SPAMS, Hexin
153 Analytical Instrument Co., Ltd.) and a scanning mobility particle sizer (SMPS, MSP
154 Corporation, USA) were used to measure the concentration of BC, the size-resolved mixing
155 state of the collected particles, and the number size distribution of submicron particles,
156 respectively. Downstream of the ambient inlet, an SMPS (Grimm 5.041, Germany), an

157 aethalometer (Model AE-31, Magee Scientific, USA), and a tapered element oscillating
158 microbalance (Model 1405, Thermo Scientific, USA) were used to determine the number
159 size distribution of submicron particles and the mass concentrations of BC and PM_{2.5},
160 respectively. During the cloud-free periods, the instruments downstream of the GCVI were
161 manually shifted and connected to the ambient PM_{2.5} inlet. During the present study, three
162 cloud events (Cloud I, II, III, each with a RH constantly above 95% for more than 12 hours)
163 were encountered and identified by the GCVI (Lin et al., 2017), as shown in Fig. 1. During
164 Cloud I and II, the cloud RES particles provided by the GCVI were measured by the
165 instruments downstream of the GCVI. During Cloud III, the cloud RES and cloud INT
166 particles were intermittently measured by these instruments at approximately one-hour
167 intervals.

168

169 **2.2 Determinations of the mass concentrations of BC**

170 The AE-31 and AE-33 measured the BC concentration at the wavelength of 880 nm,
171 which is typically represented as equivalent BC (EBC) (Petzold et al., 2013). The EBC
172 concentration reported in the present study was measured using the AE-33 described in a
173 great detail elsewhere (Drinovec et al., 2015). The limitations and uncertainties of the AE-31
174 in measuring BC and the necessary corrections were well documented (Weingartner et al.,
175 2003; Arnott et al., 2005; Backman et al., 2016). A brief description of this issue is provided
176 in the Supplement.

177

178 **2.3 Identification of BC-containing particles by the SPAMS**

179 Both the vacuum aerodynamic diameter (d_{va}) and the chemical compositions of the
180 individual particles were analyzed by the SPAMS, as briefly described in the Supplement. A
181 detailed description of the performance and the calibrations of the SPAMS can be found
182 elsewhere (Li et al., 2011a). The mass spectra for ~75000 particles with d_{va} values in the
183 range of 0.1-1.6 μm were obtained by the SPAMS over the study. The diameter is
184 represented herein as d_{va} rather than the equivalent volume diameter (d_{ve}), the conversion
185 for which can be found in the supplement (DeCarlo et al., 2004; Hu et al., 2012). An
186 adaptive resonance theory-based neural network algorithm (ART-2a) was applied to cluster
187 the individual particles based on the presence and intensities of ion peaks (Song et al., 1999)
188 with a vigilance factor of 0.7, a learning rate of 0.05, and 20 iterations. Three BC particle
189 types were obtained: the mass spectra of particles with more carbon cluster ions ($\text{C}_n^{+/-}$, $n > 6$)
190 and sulfate (BC-sul1), those with fewer carbon cluster ions ($\text{C}_n^{+/-}$, $n \leq 6$) and more intense
191 sulfate (BC-sul2), and those with an abundance of both sulfate and organics (BC-OC-sul).
192 The relative amount of OC to BC for the BC-OC-sul particles is significantly larger than
193 that in the BC-sul1 and BC-sul2 particles, as indicated in Fig. S2. Over all of the detected
194 BC-containing particles, the BC-sul2 type is the most abundant (63%) particle type,
195 followed by the BC-sul1 (21%) and BC-OC-sul (16%) types. More detailed information
196 regarding the other particle types can be found elsewhere (Lin et al., 2017).

197

198 **3 Results and Discussion**

199 During the sampling periods, the temperature and RH generally varied between -9.9 -
200 11.4 °C and 6.7 - 100% , respectively. The sampling durations for the cloud-free, cloud RES
201 and cloud INT (only detected in Cloud III) particles were approximately 109 , 123 , and 26
202 hours, respectively. The detected numbers of the cloud-free, cloud RES, and cloud INT
203 particles by the SPAMS were 48835 , 23616 , and 1063 , respectively. The average number
204 fractions of BC-containing particles in the cloud-free, cloud RES, and cloud INT particles
205 were 44% , 49% , and 53% , respectively. The number fractions of BC-containing particles
206 that were incorporated within the cloud droplets ranged between those observed at an urban
207 site (70%) in southern China (Bi et al., 2016) and those observed at a mountain site ($\sim 30\%$)
208 in Germany (Roth et al., 2016). While some mineral dust might trigger heterogeneous ice
209 nucleation at temperatures below -7 °C (Atkinson et al., 2013), this would not influence the
210 discussion on the number fraction and chemistry of the cloud RES BC-containing particles.
211 The cloud RES BC-containing particles only accounted for $\sim 0.1\%$ of all the detected ones in
212 a 2-hour window when the average temperature was ~ -7 °C.

213 Air masses from the southwestern continental and marine areas dominated throughout
214 the sampling period, carrying relatively warmer and wetter air masses that benefited the
215 formation of clouds based on the back-trajectory analysis (Lin et al., 2017). Cloud II was
216 strongly influenced by a northeastern air mass in contrast to the southwestern air mass that
217 dominated during Cloud I and III. As shown in Fig. 2, the air mass during Cloud II
218 represents relatively polluted conditions. The mass concentration of EBC during Cloud II
219 was approximately 200 ng m⁻³, which is four times that (~ 50 ng m⁻³) observed during the

220 other two events. Similarly, the number fraction of the BC-containing particles in the cloud
221 RES particles during Cloud II (~60%) was higher than those during the other two cloud
222 events (< 30%). This case might provide partial evidence for the influence of anthropogenic
223 emissions and atmospheric transport on the formation of clouds at the remote high-altitude
224 site in southern China.

225

226 **3.1 Mixing state of BC for cloud-free, residual, and interstitial particles**

227 The dominant ion peaks for the cloud-free, cloud RES, and cloud INT BC-containing
228 particles were those of carbon cluster ions ($C_n^{+/-}$, $n = 1, 2, 3, \dots$), OC fragments (m/z
229 $27[C_2H_3]^+$, $-26[CN]^-$, $37[C_3H]^+$, and $43[C_2H_3O]^+$), and secondary inorganic species, such as
230 sulfate ($-97[HSO_4]^-$), nitrate ($-62[NO_3]^-$ and $-46[NO_2]^-$), and ammonium ($18[NH_4]^+$) (Zhang
231 et al., 2014). The cloud-free BC-containing particles were internally mixed to a great extent
232 with detectable sulfate (97% by number), nitrate (50%), oxidized organics ($43[C_2H_3O]^+$,
233 72%), and/or ammonium (79%), as presented in Fig. S3. A similar mixing state of the
234 BC-containing particles has been observed at both urban and mountain sites (Moffet and
235 Prather, 2009; Li et al., 2011c; Cahill et al., 2012). The overwhelming association of BC
236 with sulfate strongly indicates a substantial influence of anthropogenic emissions of sulfate
237 precursors (e.g., SO_2) on the aging of BC (Huang and Yu, 2008; Khalizov et al., 2009; Guo
238 et al., 2012; Peng et al., 2016), which directly enhances the incorporation of BC into clouds
239 as discussed in section 3.2. Compared to the BC-containing particles at urban and suburban
240 sites that are situated close to emission sources, the relative amounts of sulfate and

241 ammonium substantially increased for those at the mountain site, as shown in Fig. S4. The
242 relative peak area (RPA) of each m/z relative to the sum of the peak areas in a mass spectrum
243 was applied herein to represent the relative amount of a species in a particle (e.g., Jeong et al.,
244 2011; Xing et al., 2011; Healy et al., 2013). The enhancement of sulfate in the atmosphere
245 above southern China is reasonable since sulfate accounts for the largest portion of the
246 compositions in this region and should be mainly associated with ammonium (Zhang et al.,
247 2013). As expected, the temporal variations of the RPAs were significantly correlated ($p <$
248 0.01) between ammonium and sulfate (Fig. S5). These species were generally regarded as
249 secondary components, and thus, such high fractions of the internal mixing state and the
250 enhancement of ammonium and sulfate at the high-altitude site demonstrates a highly aged
251 state of the BC-containing particles.

252 As shown in Fig. 3, the secondary components were enhanced in the cloud RES
253 BC-containing particles relative to the cloud INT BC-containing particles. The
254 enhancement was more obvious for sulfate rather than for ammonium, oxidized organics or
255 nitrate. The enhancement of sulfate in cloud RES particles has been broadly observed
256 (Kamphus et al., 2010; Zelenyuk et al., 2010; Hiranuma et al., 2011). A comparison of the
257 size distributions of the cloud RES and cloud INT BC-containing particles (Fig. 4) further
258 suggests that the in-cloud addition of secondary components shifted the BC-containing
259 particles towards larger sizes, which is discussed in the following section. Overall, our
260 observations suggest that the BC-containing particles were heavily coated at the
261 high-altitude site before they were incorporated into the cloud droplets and that the

262 in-cloud production of coating materials (e.g., ammonium sulfate) was present. Although
263 an abundance of BC-coated materials was also observed at Mt. Soledad by a single particle
264 soot photometer (Schroder et al., 2015), the chemical compositions of the coated materials
265 cannot be obtained to provide further information on the mixing state of BC. Our analysis
266 further reflects the importance of the chemical mixing state on the cloud processing of BC.

267 The role of the mixing state on the scavenging of the BC-containing particles was
268 further investigated through a comparison of the individual particle types of the cloud-free,
269 cloud RES, and cloud INT BC-containing particles. As shown in Fig. 5, the number
270 fraction of BC-OC-sul (~8%) was much lower in the cloud RES than those (~25%) in the
271 cloud-free and cloud INT BC-containing particles. Despite the different distributions of the
272 BC particle types, the BC-sul1 and BC-sul2 types were dominant, while the BC-OC-sul type
273 contributed only a limited fraction to the cloud RES BC-containing particles during each of
274 the cloud events. Consistently, the N_{fact} of the BC-OC-sul particles was generally lower
275 than 0.1 over the detected size range, which is much lower than those for the BC-sul1 and
276 BC-sul2 types (Fig. S6). Distinct differences in the mixing state accompanied the
277 observations of cloud RES BC-containing particles. The cloud RES BC-containing particles
278 with more sulfate and fewer organics were observed more frequently than those with more
279 organics and less sulfate (Fig. 5).

280

281 **3.2 Fractions of BC incorporated into cloud droplets**

282 **3.2.1 Size-resolved scavenging of BC-containing particles**

283 The normalized number size distributions of the cloud-free, cloud RES, and cloud INT
284 BC-containing particles are shown in Fig. 4. A representative comparison between the size
285 distributions measured by the SPAMS and the SMPS can be found in Fig. S7. While these
286 distributions do not represent the actual particle number size distributions due to the
287 decreasing detection efficiencies at smaller sizes (Allen et al., 2000; Wenzel et al., 2003; Qin
288 et al., 2006), they could reflect the importance of the particle size on the incorporation of
289 BC-containing particles into cloud droplets (Dusek et al., 2006; Matsui, 2016). The cloud
290 RES BC-containing particles had the largest size mode, followed by the cloud-free
291 BC-containing particles, with the cloud INT BC-containing particles in the smallest size
292 mode. These size distribution patterns are indicative of the preferential activation of larger
293 particles and/or the addition of secondary species during in-cloud processing, and are
294 consistent with those of previous studies (Drewnick et al., 2007; Zelenyuk et al., 2010; Roth
295 et al., 2016). As expected, the BC-containing particles were internally mixed with
296 increasingly higher intensities of sulfate, ammonium and oxidized organics with increasing
297 size (Fig. S8). These results are consistent with the observations by Healy et al. (2012) and
298 Zhang et al. (2014) inasmuch that larger BC-containing particles were more thickly coated.
299 The BC-containing particles detected by the SPAMS could track the variations of the BC
300 mass concentration in the present study based on a correlation analysis of the time series of
301 the unscaled number of BC-containing particles and the concentration of EBC (Fig. S9). A
302 detailed discussion on the comparison of these two measurements can be found in the
303 Supplement (Yu et al., 2010; Huang et al., 2011; Huang et al., 2012).

304 The size-resolved scavenged/activated fractions ($N_{f_{scav}}$) of the BC-containing particles
305 and all the detected particles were further investigated as a function of their size (Fig. 6).
306 The number fractions of the BC-containing particles incorporated into cloud droplets
307 varied between 0.05–0.45. The $N_{f_{scav}}$ generally increased with an increase in the size, and
308 those of the BC-containing particles were scavenged to a similar (or slightly lower) extent
309 as those (0.07–0.6) of all the detected particles. The size dependent scavenging of the
310 BC-containing particles is consistent with a modeling study by Matsui (2016). This
311 indicates that the coating materials on the BC-containing particles enhanced their ability to
312 act as CCN (Khalizov et al., 2009; Henning et al., 2012; Roth et al., 2016), consistent with
313 the enhanced internal mixing with secondary soluble species with an increase in the size
314 (Fig. S8) discussed above. The increase of $N_{f_{scav}}$ with the particle size also suggests that
315 nucleation scavenging is the dominant mechanism for the incorporation of BC-containing
316 particles into cloud droplets (Schroder et al., 2015). These fractions represent a rough
317 estimate because the BC-containing particles in the cloud RES and cloud INT particles were
318 measured intermittently rather than simultaneously.

319 Relatively lower scavenging efficiency (0.05–0.45) in the present study was most
320 likely attributed to less dense clouds (with a liquid water content or LWC $< 0.1 \text{ g m}^{-3}$).
321 Similarly, Matsui (2016) suggested it is not correct to assume all BC-containing particles
322 to be CCN-active in a cloud that has low maximum supersaturation (i.e., 0.1%). Generally,
323 the half activated diameter increases with decreasing LWC. Henning et al. (2002) stated
324 that particles with $d_{ve} = 700 \text{ nm}$ were only half activated with LWC $< 0.1 \text{ g m}^{-3}$, in contrast,

325 particles with $d_{ve} = \sim 100$ nm can be half activated when the LWC > 0.15 g m⁻³. Similarly,
326 Hammer et al. (2014) showed that only particles with a d_{ve} larger than 300 - 500 nm could
327 be activated under low-LWC conditions (LWC < 0.1 g m⁻³), which is a typical condition
328 for the formation of fog at the ground level. With an LWC of approximately 0.1 g m⁻³,
329 Schroder et al. (2015) reported even lower scavenged fractions (0.01–0.1) of BC-containing
330 particles at Mt. Soledad closer to the source region in California, USA. From this
331 perspective, the relatively higher scavenged fractions of the BC-containing particles in the
332 present study compared to those at Mt. Soledad (Schroder et al., 2015) could be mainly
333 attributed to the long-range transport that resulted in the highly aged BC and possibly the
334 higher LWC.

335

336 **3.2.2 Mass scavenging efficiency of EBC**

337 The concentration of EBC (5th - 95th) obtained using the AE33 for cloud-free air varied
338 over a wide range of 57 - 812 ng m⁻³ with a mean value of 418 ± 248 ng m⁻³, which accounted
339 for $\sim 2\%$ of the PM_{2.5} on average. The average concentrations of cloud RES and INT EBC
340 were 84 ± 75 , and 198 ± 125 ng m⁻³, respectively. A relatively lower contribution of EBC to
341 the aerosol population supports a substantial addition of secondary aerosols during
342 transport to the high-altitude site, given that EBC represents far more than $\sim 2\%$ of the fine
343 particles near the source regions of southern China (Lan et al., 2013; Wu et al., 2013;
344 Zhang et al., 2013). The observed relatively lower fraction of EBC is consistent with the
345 highly aged state of BC-containing particles at the high-altitude site rather than at urban

346 and suburban sites, as discussed in section 3.1. The mean concentration is much lower than
347 those observed for urban (6000 ng m⁻³) and rural (2600 ng m⁻³) areas (Huang et al., 2012)
348 in southern China. It is similar to those observed at an oceanic site (540 ng m⁻³) in southern
349 China (Wu et al., 2013) and at the high-altitude Mt. Rax site (430-720 ng m⁻³)
350 (Hitzenberger et al., 2001). It is several times higher than those at a marine boundary layer
351 site (70 ng m⁻³) in California, USA (Schroder et al., 2015), the mid-altitude regions (~60 ng
352 m⁻³) of Nova Scotia, Canada (Chýlek et al., 1996), and the high alpine Jungfrauoch station
353 (50-60 ng m⁻³) in Switzerland (Cozic et al., 2007). Additional detailed information on the
354 sampling sites and BC concentrations can be found in Table S1. These comparisons
355 suggest that anthropogenic activities have a relatively large impact on the concentration of
356 EBC at the high-altitude site.

357 It can be seen in Fig. 1 that cloud scavenging could have a strong effect on the
358 decreased particle concentrations (i.e., of EBC and PM_{2.5}). A sharp reduction in the particle
359 concentrations were observed at the beginning of the cloud events. The mass-scavenging
360 efficiency of BC ($M_{f_{scav,EBC}}$), defined as the fraction of EBC incorporated into cloud
361 droplets relative to the total amount of EBC (Cozic et al., 2007), was evaluated as

$$362 \quad M_{f_{scav,EBC}} = EBC_{RES} / (EBC_{RES} + EBC_{INT}) \times 100\% \quad (R1)$$

363 Since the EBC_{RES} and EBC_{INT} were not simultaneously obtained using the AE-33, the
364 EBC_{INT} measured concurrently by the AE-31 was applied in the calculation. The EBC
365 measured using the AE-31 is significantly correlated ($R^2 = 0.9$, $p < 0.001$) with and only
366 slightly lower than that measured by the AE-33, as shown in Fig. S10. This validates the

367 calculation in R1. The overall uncertainty in the $M_{f_{scav,EBC}}$ is within 10%, as assessed in the
368 supplement. The measurements of EBC and the sampling of the cloud RES particles were
369 regarded as the main influential factors.

370 The $M_{f_{scav,EBC}}$ ranged between 15 - 54% (5th - 95th) with an average value of
371 approximately 33%. The $M_{f_{scav,EBC}}$ in this study is within the range of those values
372 (33-54%) reported for mid-altitude (approximately 1500 m) mountain sites, generally
373 lower than those reported (45-74%) for high-altitude (approximately 3000 m) mountain
374 sites, and higher than those reported (6-15%) for ground sites (Cozic et al., 2007 and
375 references therein). The differences among the various observations are generally
376 attributed to the water content and the sizes and mixing state of the BC-containing particles
377 (Cozic et al., 2007). The $M_{f_{scav,EBC}}$ was not so different for the cloud events (Fig. S11)
378 impacted by different air masses, which is consistent with the highly aged state of the BC
379 observed in this study. These results indicate that the incorporation of BC into clouds was
380 dominantly controlled by its mixing state rather than other factors (e.g., the air mass or the
381 concentration of EBC) under low-LWC conditions (e.g., $< 0.1 \text{ g m}^{-3}$).

382

383 **4 Conclusions**

384 The influences of the size and mixing state on the incorporation of BC in clouds were
385 investigated at a remote high-altitude mountain site in southern China. On average, the mass
386 concentration of EBC was 418 ± 248 , 84 ± 75 , and $198 \pm 125 \text{ ng m}^{-3}$ for the cloud-free, cloud
387 RES, and cloud INT particles, respectively. The BC was highly aged through the

388 predominant accumulation of sulfate during transport. BC-containing particles were found
389 to be scavenged in the cloud phase to a similar extent as bulk aerosols. The size-resolved
390 scavenged fraction of BC-containing particles was estimated to be in a range of 0.05–0.45; it
391 increased with an increase in the size and was mainly controlled by the mixing state with
392 secondary soluble species. This data is restricted to particles in the size range of 0.1–1.6 μm ,
393 and thus, particles with sizes smaller than 0.1 μm that might serve as CCN are beyond the
394 scope of this study. The mass-scavenging efficiency of BC varied between 15–54% and was
395 independent of the air mass. This paper provides the first direct evidence on the substantial
396 contribution of BC-containing particles to cloud droplet residual particles in the free
397 troposphere of southern China. Our results also suggest that it might be appropriate to
398 consider BC-containing particles as a highly aged state in the free troposphere in future
399 studies. The data are also useful for constraining models used for predicting BC
400 concentrations in the free troposphere.

401

402 **Acknowledgement**

403 This work was supported by the National Key Research and Development Program of
404 China (2017YFC0210104), the National Natural Science Foundation of China (No.
405 91544101 and 41775124), the Foundation for Leading Talents of the Guangdong Province
406 Government, and the State Key Laboratory of Organic Geochemistry (SKLOGA201603A
407 and SKLOGC201604).

408 **References**

409 Allen, J. O., Ferguson, D. P., Gard, E. E., Hughes, L. S., Morrical, B. D., Kleeman, M. J.,
410 Gross, D. S., Galli, M. E., Prather, K. A., and Cass, G. R.: Particle detection efficiencies of
411 aerosol time of flight mass spectrometers under ambient sampling conditions, *Environ. Sci.*
412 *Technol.*, 34, 211-217, 2000.

413 Andreae, M. O., and Rosenfeld, D.: Aerosol–cloud–precipitation interactions. Part 1. The
414 nature and sources of cloud-active aerosols, *Earth-Sci. Rev.*, 89, 13-41,
415 doi:<http://dx.doi.org/10.1016/j.earscirev.2008.03.001>, 2008.

416 Arnott, W. P., Hamasha, K., Moosmuller, H., Sheridan, P. J., and Ogren, J. A.: Towards
417 aerosol light-absorption measurements with a 7-wavelength Aethalometer: Evaluation with a
418 photoacoustic instrument and 3-wavelength nephelometer, *Aerosol Sci. Tech.*, 39, 17-29,
419 doi:10.1080/027868290901972, 2005.

420 Atkinson, J. D., Murray, B. J., Woodhouse, M. T., Whale, T. F., Baustian, K. J., Carslaw,
421 K. S., Dobbie, S., O'Sullivan, D., and Malkin, T. L.: The importance of feldspar for ice
422 nucleation by mineral dust in mixed-phase clouds, *Nature*, 498, 355-358,
423 doi:10.1038/nature12278, 2013.

424 Backman, J., Schmeisser, L., Virkkula, A., Ogren, J. A., Asmi, E., Starkweather, S.,
425 Sharma, S., Eleftheriadis, K., Uttal, T., Jefferson, A., Bergin, M., and Makshtas, A.: On
426 Aethalometer measurement uncertainties and multiple scattering enhancement in the Arctic,
427 *Atmos. Meas. Tech. Discuss.*, 2016, 1-31, doi:10.5194/amt-2016-294, 2016.

428 Baustian, K. J., Cziczo, D. J., Wise, M. E., Pratt, K. A., Kulkarni, G., Hallar, A. G., and
429 Tolbert, M. A.: Importance of aerosol composition, mixing state, and morphology for
430 heterogeneous ice nucleation: A combined field and laboratory approach, *J. Geophys. Res.*, 117,
431 2240-2260, doi:10.1029/2011jd016784, 2012.

432 Bi, X. H., Lin, Q. H., Peng, L., Zhang, G. H., Wang, X. M., Brechtel, F. J., Chen, D. H., Li,
433 M., Peng, P. A., Sheng, G. Y., and Zhou, Z.: In situ detection of the chemistry of individual fog
434 droplet residues in the Pearl River Delta region, China, *J. Geophys. Res.-Atmos.*, 121,
435 9105-9116, doi:10.1002/2016JD024886, 2016.

436 Bond, T. C., Doherty, S. J., Fahey, D. W., Forster, P. M., Berntsen, T., DeAngelo, B. J.,
437 Flanner, M. G., Ghan, S., Karcher, B., Koch, D., Kinne, S., Kondo, Y., Quinn, P. K., Sarofim,
438 M. C., Schultz, M. G., Schulz, M., Venkataraman, C., Zhang, H., Zhang, S., Bellouin, N.,
439 Guttikunda, S. K., Hopke, P. K., Jacobson, M. Z., Kaiser, J. W., Klimont, Z., Lohmann, U.,
440 Schwarz, J. P., Shindell, D., Storelvmo, T., Warren, S. G., and Zender, C. S.: Bounding the role
441 of black carbon in the climate system: A scientific assessment, *J. Geophys. Res.-Atmos.*, 118,
442 5380-5552, doi:10.1002/Jgrd.50171, 2013.

443 Cahill, J. F., Suski, K., Seinfeld, J. H., Zaveri, R. A., and Prather, K. A.: The mixing state
444 of carbonaceous aerosol particles in northern and southern California measured during CARES
445 and CalNex 2010, *Atmos. Chem. Phys.*, 12, 10989-11002, doi:10.5194/acp-12-10989-2012,
446 2012.

447 Chýlek, P., Banic, C. M., Johnson, B., Damiano, P. A., Isaac, G. A., Leaitch, W. R., Liu, P.
448 S. K., Boudala, F. S., Winter, B., and Ngo, D.: Black carbon: Atmospheric concentrations and
449 cloud water content measurements over southern Nova Scotia, *J. Geophys. Res.-Atmos.*, 101,
450 29105-29110, doi:10.1029/95JD03433, 1996.

451 Ching, J., Riemer, N., and West, M.: Impacts of black carbon mixing state on black carbon
452 nucleation scavenging: Insights from a particle-resolved model, *J. Geophys. Res.-Atmos.*, 117,
453 1-21, 2012.

454 Cozic, J., Verheggen, B., Mertes, S., Connolly, P., Bower, K., Petzold, A., Baltensperger,
455 U., and Weingartner, E.: Scavenging of black carbon in mixed phase clouds at the high alpine
456 site Jungfraujoch, *Atmos. Chem. Phys.*, 7, 1797-1807, 2007.

457 Cubison, M. J., Ervens, B., Feingold, G., Docherty, K. S., Ulbrich, I. M., Shields, L.,
458 Prather, K., Hering, S., and Jimenez, J. L.: The influence of chemical composition and mixing
459 state of Los Angeles urban aerosol on CCN number and cloud properties, *Atmos. Chem. Phys.*,
460 8, 5649-5667, 2008.

461 DeCarlo, P. F., Slowik, J. G., Worsnop, D. R., Davidovits, P., and Jimenez, J. L.: Particle
462 morphology and density characterization by combined mobility and aerodynamic diameter

463 measurements. Part 1: Theory, *Aerosol Sci. Tech.*, 38, 1185-1205,
464 doi:10.1080/027868290903907, 2004.

465 Drewnick, F., Schneider, J., Hings, S. S., Hock, N., Noone, K., Targino, A., Weimer, S.,
466 and Borrmann, S.: Measurement of ambient, interstitial, and residual aerosol particles on a
467 mountaintop site in central Sweden using an aerosol mass spectrometer and a CVI, *J. Atmos.*
468 *Chem.*, 56, 1-20, doi:10.1007/s10874-006-9036-8, 2007.

469 Drinovec, L., Močnik, G., Zotter, P., Prévôt, A. S. H., Ruckstuhl, C., Coz, E., Rupakheti,
470 M., Sciare, J., Müller, T., Wiedensohler, A., and Hansen, A. D. A.: The "dual-spot"
471 Aethalometer: an improved measurement of aerosol black carbon with real-time loading
472 compensation, *Atmos. Meas. Tech.*, 8, 1965-1979, doi:10.5194/amt-8-1965-2015, 2015.

473 Dusek, U., Frank, G. P., Hildebrandt, L., Curtius, J., Schneider, J., Walter, S., Chand, D.,
474 Drewnick, F., Hings, S., Jung, D., Borrmann, S., and Andreae, M. O.: Size matters more than
475 chemistry for cloud-nucleating ability of aerosol particles, *Science*, 312, 1375-1378,
476 doi:10.1126/science.1125261, 2006.

477 Furutani, H., Dall'osto, M., Roberts, G. C., and Prather, K. A.: Assessment of the relative
478 importance of atmospheric aging on CCN activity derived from field observations, *Atmos.*
479 *Environ.*, 42, 3130-3142, doi:10.1016/j.atmosenv.2007.09.024, 2008.

480 Guo, J., Wang, Y., Shen, X. H., Wang, Z., Lee, T., Wang, X. F., Li, P. H., Sun, M. H.,
481 Collett, J. L., Wang, W. X., and Wang, T.: Characterization of cloud water chemistry at Mount
482 Tai, China: Seasonal variation, anthropogenic impact, and cloud processing, *Atmos. Environ.*,
483 60, 467-476, doi:10.1016/j.atmosenv.2012.07.016, 2012.

484 Hammer, E., Gysel, M., Roberts, G. C., Elias, T., Hofer, J., Hoyle, C. R., Bukowiecki, N.,
485 Dupont, J. C., Burnet, F., Baltensperger, U., and Weingartner, E.: Size-dependent particle
486 activation properties in fog during the ParisFog 2012/13 field campaign, *Atmos. Chem. Phys.*,
487 14, 10517-10533, doi:10.5194/acp-14-10517-2014, 2014.

488 Hayden, K. L., Macdonald, A. M., Gong, W., Toom-Sauntry, D., Anlauf, K. G., Leithead,
489 A., Li, S. M., Leaitch, W. R., and Noone, K.: Cloud processing of nitrate, *J. Geophys.*
490 *Res.-Atmos.*, 113, 1-18, doi:10.1029/2007jd009732, 2008.

491 Healy, R. M., Sciare, J., Poulain, L., Kamili, K., Merkel, M., Muller, T., Wiedensohler, A.,
492 Eckhardt, S., Stohl, A., Sarda-Esteve, R., McGillicuddy, E., O'Connor, I. P., Sodeau, J. R., and
493 Wenger, J. C.: Sources and mixing state of size-resolved elemental carbon particles in a
494 European megacity: Paris, *Atmos. Chem. Phys.*, 12, 1681-1700,
495 doi:10.5194/acp-12-1681-2012, 2012.

496 Healy, R. M., Sciare, J., Poulain, L., Crippa, M., Wiedensohler, A., Prevot, A. S. H.,
497 Baltensperger, U., Sarda-Esteve, R., McGuire, M. L., Jeong, C. H., McGillicuddy, E.,
498 O'Connor, I. P., Sodeau, J. R., Evans, G. J., and Wenger, J. C.: Quantitative determination of
499 carbonaceous particle mixing state in Paris using single-particle mass spectrometer and aerosol
500 mass spectrometer measurements, *Atmos. Chem. Phys.*, 13, 9479-9496,
501 doi:10.5194/acp-13-9479-2013, 2013.

502 Heintzenberg, J., Cereceda-Balic, F., Vidal, V., and Leck, C.: Scavenging of black carbon
503 in Chilean coastal fogs, *Sci. Total. Environ.*, 541, 341-347, 2016.

504 Henning, S., Weingartner, E., Schmidt, S., Wendisch, M., Gaggeler, H. W., and
505 Baltensperger, U.: Size-dependent aerosol activation at the high-alpine site Jungfraujoch (3580
506 m asl), *Tellus B*, 54, 82-95, 2002.

507 Henning, S., Ziese, M., Kiselev, A., Saathoff, H., Mohler, O., Mentel, T. F., Buchholz, A.,
508 Spindler, C., Michaud, V., Monier, M., Sellegri, K., and Stratmann, F.: Hygroscopic growth
509 and droplet activation of soot particles: uncoated, succinic or sulfuric acid coated, *Atmos.*
510 *Chem. Phys.*, 12, 4525-4537, doi:10.5194/acp-12-4525-2012, 2012.

511 Herrmann, H., Schaefer, T., Tilgner, A., Styler, S. A., Weller, C., Teich, M., and Otto, T.:
512 Tropospheric Aqueous-Phase Chemistry: Kinetics, Mechanisms, and Its Coupling to a
513 Changing Gas Phase, *Chem. Rev.*, 115, 4259-4334, doi:10.1021/cr500447k, 2015.

514 Hiranuma, N., Kohn, M., Pekour, M. S., Nelson, D. A., Shilling, J. E., and Cziczo, D. J.:
515 Droplet activation, separation, and compositional analysis: laboratory studies and atmospheric
516 measurements, *Atmos. Meas. Tech.*, 4, 2333-2343, doi:10.5194/amt-4-2333-2011, 2011.

517 Hitzenberger, R., Berner, A., Glebl, H., Drobesh, K., Kasper-Giebl, A., Loefflund, M.,
518 Urban, H., and Puxbaum, H.: Black carbon (BC) in alpine aerosols and cloud water -
519 concentrations and scavenging efficiencies, *Atmos. Environ.*, 35, 5135-5141, 2001.

520 Hu, M., Peng, J. F., Sun, K., Yue, D. L., Guo, S., Wiedensohler, A., and Wu, Z. J.:
521 Estimation of Size-Resolved Ambient Particle Density Based on the Measurement of Aerosol
522 Number, Mass, and Chemical Size Distributions in the Winter in Beijing, *Environ. Sci.*
523 *Technol.*, 46, 9941-9947, doi:10.1021/Es204073t, 2012.

524 Huang, X. F., and Yu, J. Z.: Size distributions of elemental carbon in the atmosphere of a
525 coastal urban area in South China: characteristics, evolution processes, and implications for the
526 mixing state, *Atmos. Chem. Phys.*, 8, 5843-5853, 2008.

527 Huang, X. F., Gao, R. S., Schwarz, J. P., He, L. Y., Fahey, D. W., Watts, L. A.,
528 McComiskey, A., Cooper, O. R., Sun, T. L., Zeng, L. W., Hu, M., and Zhang, Y. H.: Black
529 carbon measurements in the Pearl River Delta region of China, *J. Geophys. Res.*, 116, 445-451,
530 doi:10.1029/2010jd014933, 2011.

531 Huang, X. F., Sun, T. L., Zeng, L. W., Yu, G. H., and Luan, S. J.: Black carbon aerosol
532 characterization in a coastal city in South China using a single particle soot photometer, *Atmos.*
533 *Environ.*, 51, 21-28, doi:10.1016/j.atmosenv.2012.01.056, 2012.

534 Jeong, C. H., McGuire, M. L., Godri, K. J., Slowik, J. G., Rehbein, P. J. G., and Evans, G.
535 J.: Quantification of aerosol chemical composition using continuous single particle
536 measurements, *Atmos. Chem. Phys.*, 11, 7027-7044, doi:10.5194/acp-11-7027-2011, 2011.

537 Kammermann, L., Gysel, M., Weingartner, E., Herich, H., Cziczo, D. J., Holst, T.,
538 Svenningsson, B., Arneth, A., and Baltensperger, U.: Subarctic atmospheric aerosol
539 composition: 3. Measured and modeled properties of cloud condensation nuclei, *J. Geophys.*
540 *Res.-Atmos.*, 115, 288-303, doi:10.1029/2009jd012447, 2010.

541 Kamphus, M., Ettner-Mahl, M., Klimach, T., Drewnick, F., Keller, L., Cziczo, D. J.,
542 Mertes, S., Borrmann, S., and Curtius, J.: Chemical composition of ambient aerosol, ice
543 residues and cloud droplet residues in mixed-phase clouds: single particle analysis during the

544 Cloud and Aerosol Characterization Experiment (CLACE 6), *Atmos. Chem. Phys.*, 10,
545 8077-8095, doi:10.5194/acp-10-8077-2010, 2010.

546 Khalizov, A. F., Zhang, R. Y., Zhang, D., Xue, H. X., Pagels, J., and McMurry, P. H.:
547 Formation of highly hygroscopic soot aerosols upon internal mixing with sulfuric acid vapor, *J.*
548 *Geophys. Res.-Atmos.*, 114, 730-734, doi:10.1029/2008jd010595, 2009.

549 Lambe, A. T., Ahern, A. T., Wright, J. P., Croasdale, D. R., Davidovits, P., and Onasch, T.
550 B.: Oxidative aging and cloud condensation nuclei activation of laboratory combustion soot, *J.*
551 *Aerosol Sci.*, 79, 31-39, 2015.

552 Lan, Z. J., Huang, X. F., Yu, K. Y., Sun, T. L., Zeng, L. W., and Hu, M.: Light absorption
553 of black carbon aerosol and its enhancement by mixing state in an urban atmosphere in South
554 China, *Atmos. Environ.*, 69, 118-123, doi:10.1016/j.atmosenv.2012.12.009, 2013.

555 Li, L., Huang, Z. X., Dong, J. G., Li, M., Gao, W., Nian, H. Q., Fu, Z., Zhang, G. H., Bi, X.
556 H., Cheng, P., and Zhou, Z.: Real time bipolar time-of-flight mass spectrometer for analyzing
557 single aerosol particles, *Intl. J. Mass. Spectrom.*, 303, 118-124, doi:10.1016/j.ijms.2011.01.017,
558 2011a.

559 Li, W. J., Li, P. R., Sun, G. D., Zhou, S. Z., Yuan, Q., and Wang, W. X.: Cloud residues
560 and interstitial aerosols from non-precipitating clouds over an industrial and urban area in
561 northern China, *Atmos. Environ.*, 45, 2488-2495, doi:10.1016/j.atmosenv.2011.02.044, 2011b.

562 Li, W. J., Zhou, S. Z., Wang, X. F., Xu, Z., Yuan, C., Yu, Y. C., Zhang, Q. Z., and Wang,
563 W. X.: Integrated evaluation of aerosols from regional brown hazes over northern China in
564 winter: Concentrations, sources, transformation, and mixing states, *J. Geophys. Res.*, 116, 1-11,
565 doi:10.1029/2010jd015099, 2011c.

566 Lin, Q., Zhang, G., Peng, L., Bi, X., Wang, X., Brechtel, F. J., Li, M., Chen, D., Peng, P.,
567 Sheng, G., and Zhou, Z.: In situ chemical composition measurement of individual cloud residue
568 particles at a mountain site, southern China, *Atmos. Chem. Phys.*, 17, 8473-8488,
569 doi:10.5194/acp-17-8473-2017, 2017.

570 Matsui, H.: Black carbon simulations using a size- and mixing-state-resolved
571 three-dimensional model: 2. Aging timescale and its impact over East Asia, *J. Geophys.*
572 *Res.-Atmos.*, 121, 1808-1821, doi:10.1002/2015jd023999, 2016.

573 McFiggans, G., Artaxo, P., Baltensperger, U., Coe, H., Facchini, M. C., Feingold, G.,
574 Fuzzi, S., Gysel, M., Laaksonen, A., Lohmann, U., Mentel, T. F., Murphy, D. M., O'Dowd, C.
575 D., Snider, J. R., and Weingartner, E.: The effect of physical and chemical aerosol properties on
576 warm cloud droplet activation, *Atmos. Chem. Phys.*, 6, 2593-2649, 2006.

577 Moffet, R. C., and Prather, K. A.: In-situ measurements of the mixing state and optical
578 properties of soot with implications for radiative forcing estimates, *Proc. Natl. Acad. Sci. USA*,
579 106, 11872-11877, doi:10.1073/pnas.0900040106, 2009.

580 Peng, J. F., Hu, M., Guo, S., Du, Z. F., Zheng, J., Shang, D. J., Zamora, M. L., Zeng, L. M.,
581 Shao, M., Wu, Y. S., Zheng, J., Wang, Y., Glen, C. R., Collins, D. R., Molina, M. J., and Zhang,
582 R. Y.: Markedly enhanced absorption and direct radiative forcing of black carbon under
583 polluted urban environments, *Proc. Natl. Acad. Sci. USA*, 113, 4266-4271,
584 doi:10.1073/pnas.1602310113, 2016.

585 Petzold, A., Ogren, J. A., Fiebig, M., Laj, P., Li, S. M., Baltensperger, U., Holzer-Popp, T.,
586 Kinne, S., Pappalardo, G., Sugimoto, N., Wehrli, C., Wiedensohler, A., and Zhang, X. Y.:
587 Recommendations for reporting "black carbon" measurements, *Atmos. Chem. Phys.*, 13,
588 8365-8379, 2013.

589 Qin, X. Y., Bhawe, P. V., and Prather, K. A.: Comparison of two methods for obtaining
590 quantitative mass concentrations from aerosol time-of-flight mass spectrometry measurements,
591 *Anal. Chem.*, 78, 6169-6178, doi:10.1021/ac060395q, 2006.

592 Roth, A., Schneider, J., Klimach, T., Mertes, S., van Pinxteren, D., Herrmann, H., and
593 Borrmann, S.: Aerosol properties, source identification, and cloud processing in orographic
594 clouds measured by single particle mass spectrometry on a central European mountain site
595 during HCCT-2010, *Atmos. Chem. Phys.*, 16, 505-524, doi:10.5194/acp-16-505-2016, 2016.

596 Schroder, J. C., Hanna, S. J., Modini, R. L., Corrigan, A. L., Kreidenwies, S. M.,
597 Macdonald, A. M., Noone, K. J., Russell, L. M., Leitch, W. R., and Bertram, A. K.:

598 Size-resolved observations of refractory black carbon particles in cloud droplets at a marine
599 boundary layer site, *Atmos. Chem. Phys.*, 15, 1367-1383, doi:10.5194/acp-15-1367-2015,
600 2015.

601 Sellegri, K., Laj, P., Dupuy, R., Legrand, M., Preunkert, S., and Putaud, J. P.:
602 Size-dependent scavenging efficiencies of multicomponent atmospheric aerosols in clouds, *J.*
603 *Geophys. Res.-Atmos.*, 108, 651-663, 2003.

604 Shingler, T., Dey, S., Sorooshian, A., Brechtel, F. J., Wang, Z., Metcalf, A., Coggon, M.,
605 Mulmenstadt, J., Russell, L. M., Jonsson, H. H., and Seinfeld, J. H.: Characterisation and
606 airborne deployment of a new counterflow virtual impactor inlet, *Atmos. Meas. Tech.*, 5,
607 1259-1269, doi:10.5194/amt-5-1259-2012, 2012.

608 Song, X. H., Hopke, P. K., Fergenson, D. P., and Prather, K. A.: Classification of single
609 particles analyzed by ATOFMS using an artificial neural network, *ART-2A, Anal. Chem.*, 71,
610 860-865, 1999.

611 Sorooshian, A., Wang, Z., Coggon, M. M., Jonsson, H. H., and Ervens, B.: Observations
612 of Sharp Oxalate Reductions in Stratocumulus Clouds at Variable Altitudes: Organic Acid and
613 Metal Measurements During the 2011 E-PEACE Campaign, *Environ. Sci. Technol.*, 47,
614 7747-7756, doi:10.1021/es4012383, 2013.

615 Straub, D. J., Hutchings, J. W., and Herckes, P.: Measurements of fog composition at a
616 rural site, *Atmos. Environ.*, 47, 195-205, doi:10.1016/j.atmosenv.2011.11.014, 2012.

617 van Pinxteren, D., Fomba, K. W., Mertes, S., Muller, K., Spindler, G., Schneider, J., Lee,
618 T., Collett, J. L., and Herrmann, H.: Cloud water composition during HCCT-2010: Scavenging
619 efficiencies, solute concentrations, and droplet size dependence of inorganic ions and dissolved
620 organic carbon, *Atmos. Chem. Phys.*, 16, 3185-3205, doi:10.5194/acp-16-3185-2016, 2016.

621 Wang, Z., Wang, T., Guo, J., Gao, R., Xue, L. K., Zhang, J. M., Zhou, Y., Zhou, X. H.,
622 Zhang, Q. Z., and Wang, W. X.: Formation of secondary organic carbon and cloud impact on
623 carbonaceous aerosols at Mount Tai, North China, *Atmos. Environ.*, 46, 516-527,
624 doi:10.1016/j.atmosenv.2011.08.019, 2012.

625 Weingartner, E., Saathoff, H., Schnaiter, M., Streit, N., Bitnar, B., and Baltensperger, U.:
626 Absorption of light by soot particles: determination of the absorption coefficient by means of
627 aethalometers, *J. Aerosol Sci.*, 34, 1445-1463,
628 doi:[http://dx.doi.org/10.1016/S0021-8502\(03\)00359-8](http://dx.doi.org/10.1016/S0021-8502(03)00359-8), 2003.

629 Wenzel, R. J., Liu, D. Y., Edgerton, E. S., and Prather, K. A.: Aerosol time-of-flight mass
630 spectrometry during the Atlanta Supersite Experiment: 2. Scaling procedures, *J. Geophys.*
631 *Res.-Atmos.*, 108, 447-457, doi:10.1029/2001jd001563, 2003.

632 Wu, D., Wu, C., Liao, B., Chen, H., Wu, M., Li, F., Tan, H., Deng, T., Li, H., Jiang, D.,
633 and Yu, J. Z.: Black carbon over the South China Sea and in various continental locations in
634 South China, *Atmos. Chem. Phys.*, 13, 12257-12270, doi:10.5194/acp-13-12257-2013, 2013.

635 Xing, J. H., Takahashi, K., Yabushita, A., Kinugawa, T., Nakayama, T., Matsumi, Y.,
636 Tonokura, K., Takami, A., Imamura, T., Sato, K., Kawasaki, M., Hikida, T., and Shimono, A.:
637 Characterization of Aerosol Particles in the Tokyo Metropolitan Area using Two Different
638 Particle Mass Spectrometers, *Aerosol Sci. Tech.*, 45, 315-326,
639 doi:10.1080/02786826.2010.533720, 2011.

640 Yu, H., Wu, C., Wu, D., and Yu, J. Z.: Size distributions of elemental carbon and its
641 contribution to light extinction in urban and rural locations in the pearl river delta region, China,
642 *Atmos. Chem. Phys.*, 10, 5107-5119, doi:10.5194/acp-10-5107-2010, 2010.

643 Zaveri, R. A., Barnard, J. C., Easter, R. C., Riemer, N., and West, M.: Particle-resolved
644 simulation of aerosol size, composition, mixing state, and the associated optical and cloud
645 condensation nuclei activation properties in an evolving urban plume, *J. Geophys. Res.-Atmos.*,
646 115, 1383-1392, doi:10.1029/2009jd013616, 2010.

647 Zelenyuk, A., Imre, D., Earle, M., Easter, R., Korolev, A., Leitch, R., Liu, P., Macdonald,
648 A. M., Ovchinnikov, M., and Strapp, W.: In Situ Characterization of Cloud Condensation
649 Nuclei, Interstitial, and Background Particles Using the Single Particle Mass Spectrometer,
650 SPLAT II, *Anal. Chem.*, 82, 7943-7951, doi:10.1021/Ac1013892, 2010.

651 Zhang, G., Lin, Q., Peng, L., Yang, Y., Fu, Y., Bi, X., Li, M., Chen, D., Chen, J., Cai, Z.,
652 Wang, X., Peng, P., Sheng, G., and Zhou, Z.: Insight into the in-cloud formation of oxalate

653 based on in situ measurement by single particle mass spectrometry, *Atmos. Chem. Phys.*
654 *Discuss.*, 2017, 1-39, doi:10.5194/acp-2017-763, 2017.

655 Zhang, G. H., Bi, X. H., Chan, L. Y., Li, L., Wang, X. M., Feng, J. L., Sheng, G. Y., Fu, J.
656 M., Li, M., and Zhou, Z.: Enhanced trimethylamine-containing particles during fog events
657 detected by single particle aerosol mass spectrometry in urban Guangzhou, China, *Atmos.*
658 *Environ.*, 55, 121-126, doi:10.1016/j.atmosenv.2012.03.038, 2012.

659 Zhang, G. H., Bi, X. H., Chan, L. Y., Wang, X. M., Sheng, G. Y., and Fu, J. M.:
660 Size-segregated chemical characteristics of aerosol during haze in an urban area of the Pearl
661 River Delta region, China, *Urban Climate*, 4, 74-84, doi:10.1016/j.uclim.2013.05.002, 2013.

662 Zhang, G. H., Bi, X. H., He, J. J., Chen, D. H., Chan, L. Y., Xie, G. W., Wang, X. M.,
663 Sheng, G. Y., Fu, J. M., and Zhou, Z.: Variation of secondary coatings associated with
664 elemental carbon by single particle analysis, *Atmos. Environ.*, 92, 162-170,
665 doi:10.1016/j.atmosenv.2014.04.018, 2014.

666 Zhou, Y., Wang, T., Gao, X. M., Xue, L. K., Wang, X. F., Wang, Z., Gao, J. A., Zhang, Q.
667 Z., and Wang, W. X.: Continuous observations of water-soluble ions in PM_{2.5} at Mount Tai
668 (1534 m.a.s.l.) in central-eastern China, *J. Atmos. Chem.*, 64, 107-127, 2009.

669 Zuberi, B., Johnson, K. S., Aleks, G. K., Molina, L. T., and Laskin, A.: Hydrophilic
670 properties of aged soot, *Geophys. Res. Lett.*, 32, 67-106, doi:10.1029/2004gl021496, 2005.

671

672 **Figure captions**

673 Fig. 1. Temporal profiles (with a 1 hour resolution) of PM_{2.5}, EBC mass concentrations,
674 number of BC-containing particles by SPAMS, RH and visibility. Three cloud events are
675 illustrated with black bars above the figure. PM_{2.5} during the cloud events corresponded to the
676 cloud INT particles. EBC and number of BC-containing particles data were shown for all
677 categories, including the cloud-free, cloud RES, and cloud INT particles. The cloud INT
678 particles were only measured during Cloud III.

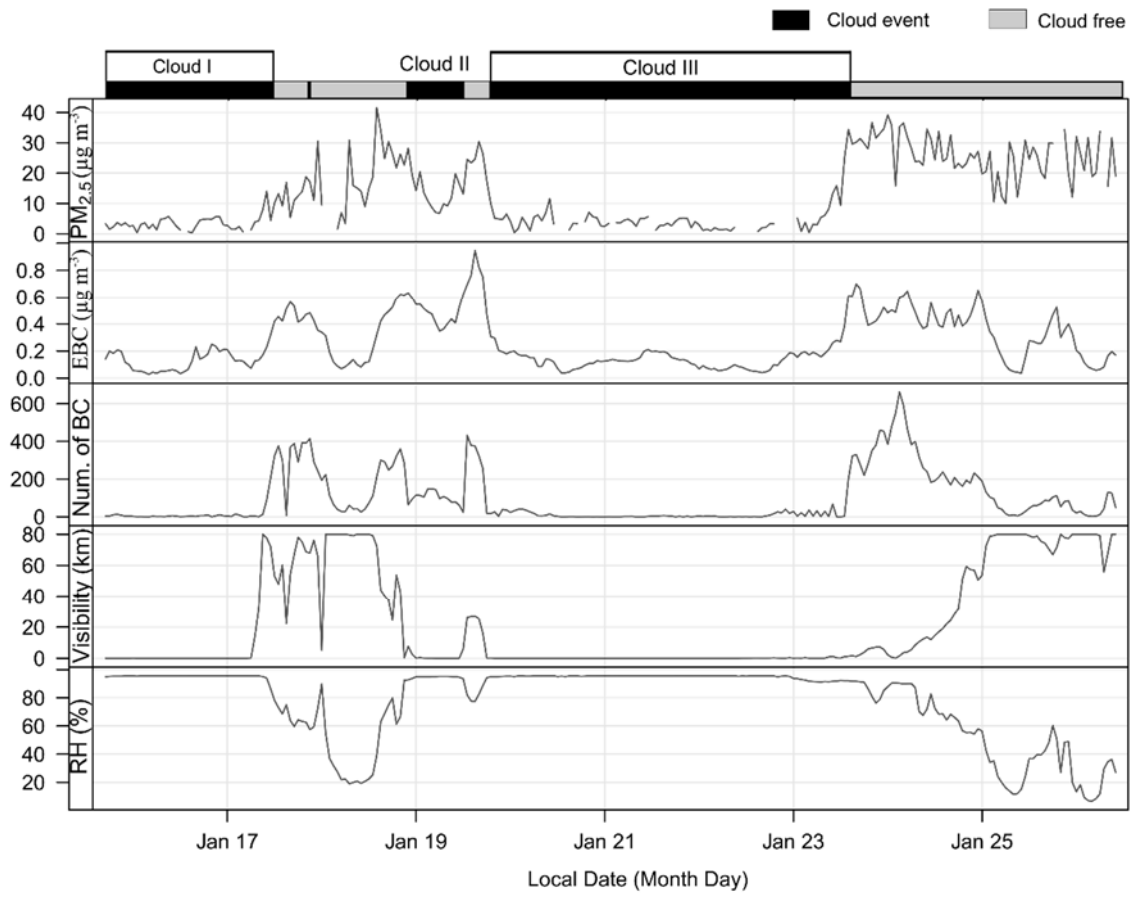
679 Fig. 2. Box and whisker plots of (a) concentration of EBC and (b) number fraction of
680 BC-containing particles for each cloud event. In a box and whisker plot, the lower, median
681 and upper lines of the box denote the 25th, 50th, and 75th percentiles, respectively, and the
682 lower and upper edges of the whisker denote the 10th and 90th percentiles, respectively.

683 Fig. 3. (a) Average mass spectrum of the cloud RES BC-containing particles, and (b) the
684 RPA ratios of ammonium, sulfate, nitrate, oxidized organic markers, and other organic
685 markers (i.e., m/z 27[C₂H₃]⁺, -26[CN]⁻, 37[C₃H]⁺, 50[C₄H₂]⁺, 51[C₄H₃]⁺, 61[C₅H]⁺, and
686 63[C₅H₃]⁺) to BC (carbon ion clusters (C_n^{+/-}, n ≤ 5)), and the RPAs of BC for the cloud RES
687 and INT particles, respectively. Error bars represent the standard deviation in the hourly
688 average RPA or the RPA ratios within a 95% confidence interval.

689 Fig. 4. Normalized SPAMS particle count (to average count) over the measured size
690 range for the cloud-free, cloud INT, and cloud RES BC-containing particles, respectively. The
691 data were averaged throughout the sampling period.

692 Fig. 5. (a) Number fraction of each BC particle type in the cloud-free, INT, and RES
693 BC-containing particles, and (b) the number fraction of each BC particle type in the cloud
694 RES BC-containing particles separated for the three cloud events.

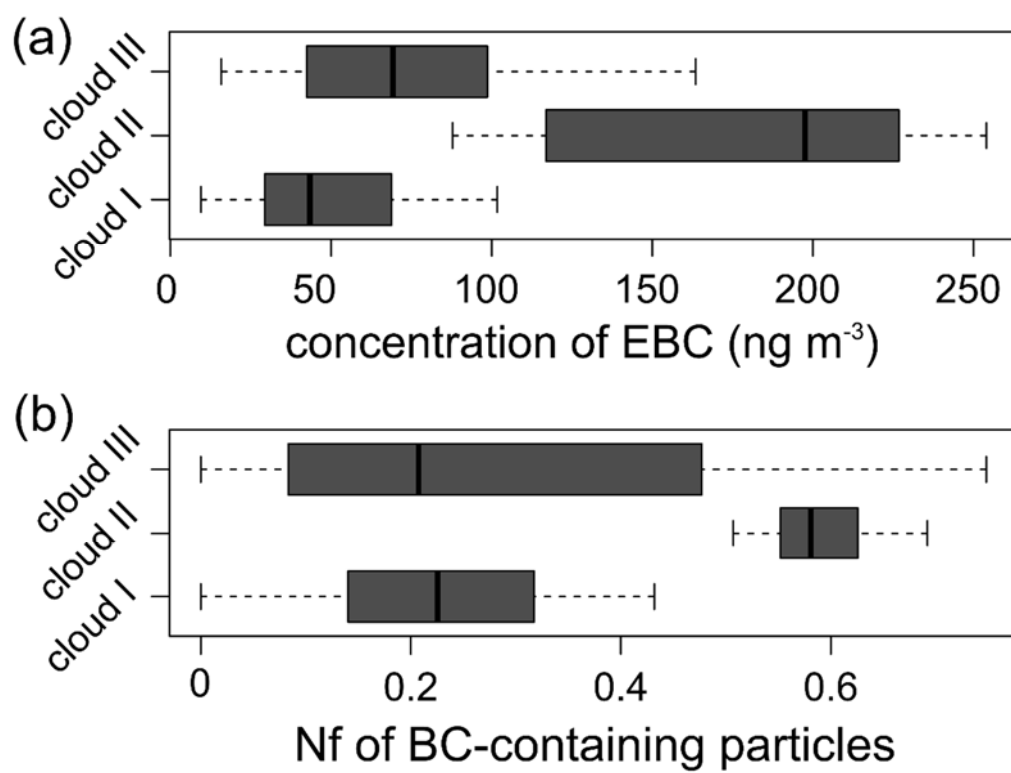
695 Fig. 6. Size-resolved $N_{f_{scav}}$ estimated for the BC-containing particles and all the detected
696 particles. The $N_{f_{scav}}$ is calculated as the ratio of the average number size distribution for the
697 cloud RES particles to the sum of the average number size distributions for the cloud RES and
698 INT particles. Errors were estimated assuming that the particle numbers detected by the
699 SPAMS follow a Poisson distribution.



700

701

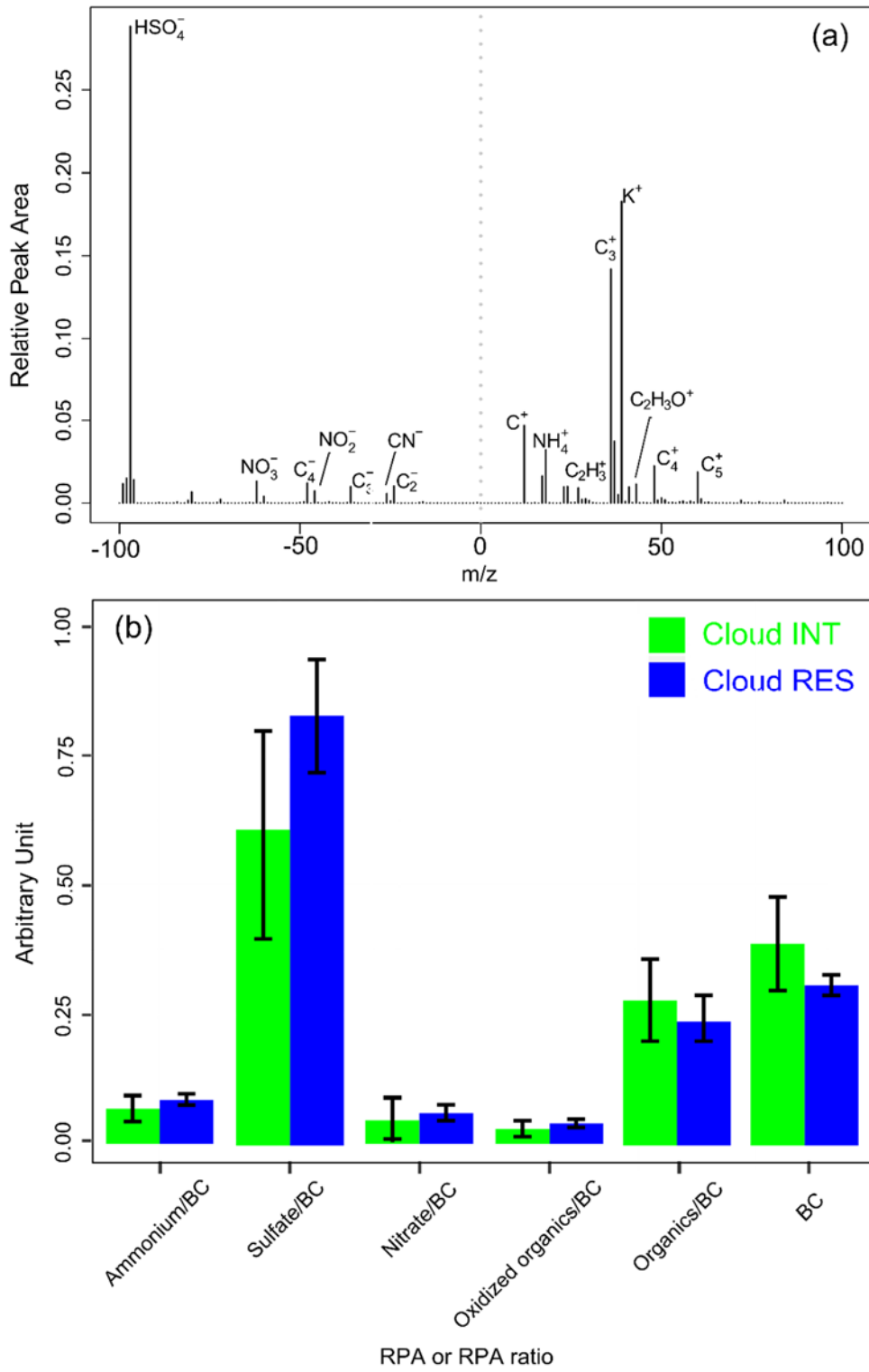
Fig. 1.



702

703

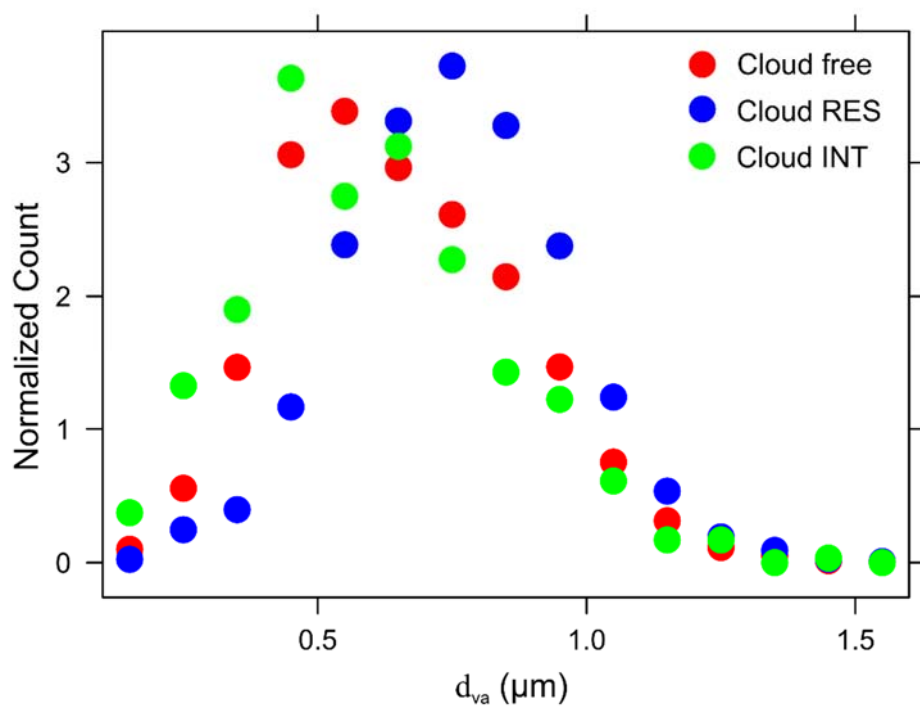
Fig. 2.



704

705

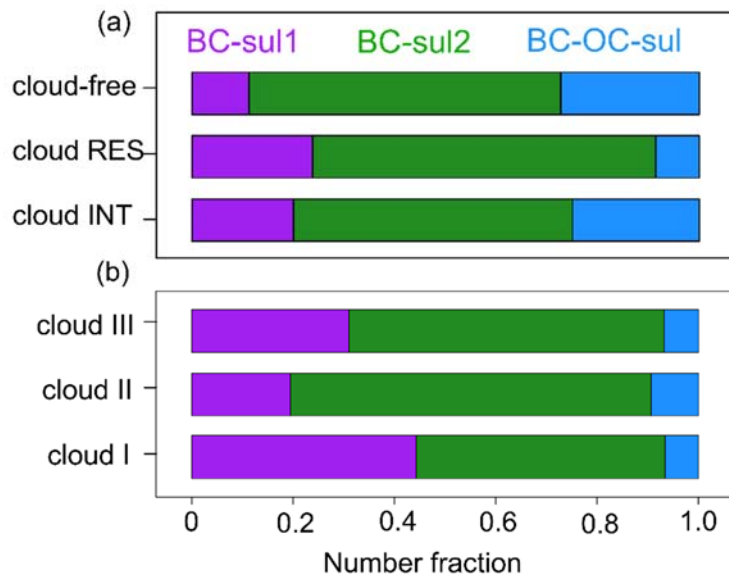
Fig. 3.



706

707

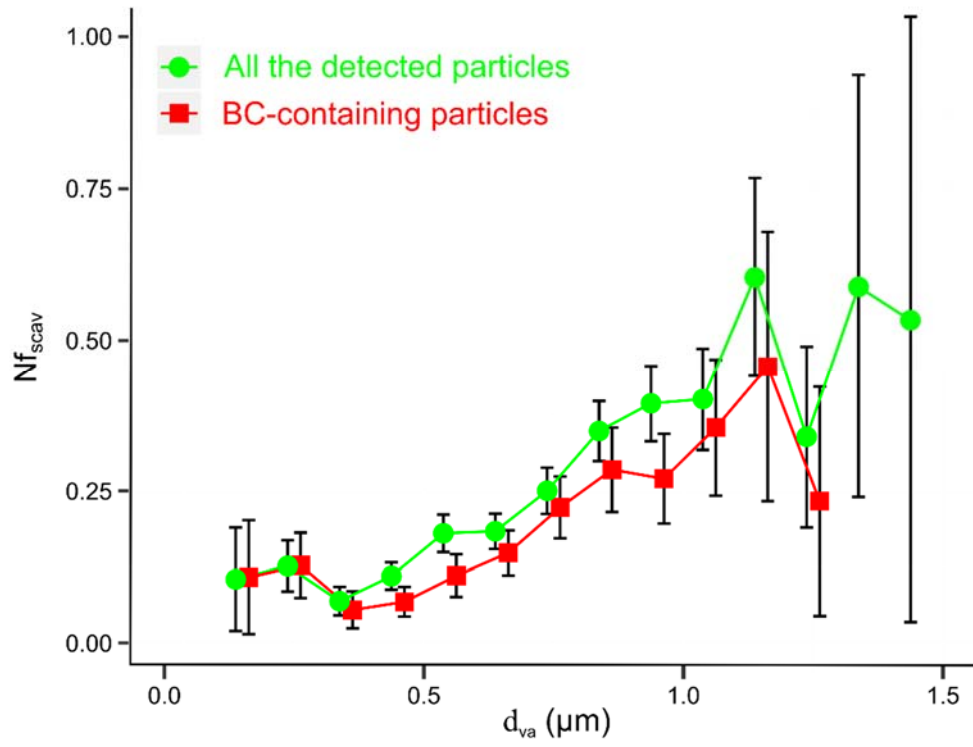
Fig. 4.



708

709

Fig. 5.



710

711

Fig. 6.